

## Fragmentation of silicon microclusters: A molecular-dynamics study

B. P. Feuston

*Department of Physics, University of Cincinnati, Cincinnati, Ohio 45221  
and Materials Science Division, Argonne National Laboratory, Argonne, Illinois 60439-4843*

R. K. Kalia and P. Vashishta\*

*Materials Science Division, Argonne National Laboratory, Argonne, Illinois 60439-4843*

(Received 8 September 1986; revised manuscript received 24 November 1986)

A detailed molecular-dynamics (MD) study has been performed to (i) enumerate ground-state and finite-temperature structures and (ii) investigate the nature of fragmentation for  $\text{Si}_N$  clusters ( $N=2-14$ ), using the Stillinger-Weber three-body interaction potential. We investigate all underlying mechanically stable structures visited by the system in the equilibrium state. Results indicate that the presence of magic numbers, unusually stable finite-temperature clusters  $\text{Si}_4$ ,  $\text{Si}_6$ , and  $\text{Si}_{10}$  as determined by the photofragmentation experiment of Bloomfield, Freeman, and Brown is dependent upon the topology and energetics of high-energy bound structures rather than upon the structure and ground-state energies at zero temperature.

### I. INTRODUCTION

Recent work on metallic<sup>1-4</sup> and inert-gas clusters<sup>5-9</sup> has stimulated a growing interest in the geometrical arrangements and electronic configurations of group-IV microclusters.<sup>10-16</sup> Inert gases are known to form predominantly 13-, 55-, etc., atom clusters which are explained by stable icosahedral packing.<sup>17</sup> Unusually stable 4-, 6-, and 10-atom microclusters, referred to as "magic numbers," are found for covalently bonded semiconductors such as silicon<sup>12</sup> and germanium.<sup>13</sup> Due to strong  $\pi$  bonding, carbon clusters exhibit chainlike structures with their own set of magic numbers.<sup>18</sup> In the photofragmentation experiment on ionized silicon, Bloomfield, Freeman, and Brown<sup>12</sup> (BFB) determined relative cross sections and individual fragmentation channels for  $N=2-12$ . They reported relatively low total photofragmentation cross sections for  $\text{Si}_4^+$ ,  $\text{Si}_6^+$ , and  $\text{Si}_{10}^+$  clusters in addition to an abundance of  $\text{Si}_6^+$ ,  $\text{Si}_{10}^+$  from the fragmentation of  $\text{Si}_{7-11}^+$ ,  $\text{Si}_{12}^+$ , respectively, indicating the possible existence of particularly stable and compact structures for  $\text{Si}_6^+$ ,  $\text{Si}_{10}^+$ , and possibly  $\text{Si}_4^+$ . Fragmentation occurred by exposing the mass selected, ionized cluster to an intense beam of pulsed-laser radiation. The size distribution of the resulting fragments was reported to depend critically on the overlap between the laser beam and cluster. The clusters dissociated at temperatures on the order of the melting temperature, well above the  $T=0$  ground state, and the fragmentation spectra were shown to be temperature dependent. An early sublimation study on silicon by Honig<sup>10</sup> supports the common occurrence of  $\text{Si}_6^+$  and reports the dissociation energy of the  $\text{Si}_2$  dimer to be 3.25 eV/atom.

In carrying out a theoretical calculation to explain these results, one wants to determine for each cluster considered (i) all mechanically stable configurations at  $T=0$ , (ii) the most probable configurations at finite temperatures, (iii) the temperature at which the cluster would fragment into

two or more smaller clusters, (iv) the fragmentation spectra, and (v) the configurations from which it is most likely to fragment.

Several models<sup>12</sup> and theoretical calculations<sup>15,16,19,20</sup> have been offered thus far to explain the magic numbers obtained from the photofragmentation experiment on Si. Bloomfield *et al.*<sup>12</sup> proposed a simple model, consistent with the data, of silicon clusters reconstructed from microcrystals of the diamond lattice. The triangle, rhombus, and trigonal bipyramid form the compact geometries for  $N=3-5$ . For larger clusters, two geometries essential to the model are the reconstructed six-atom "chair" ring and ten-atom "adamantane cage" subunits of the diamond structure. Large clusters are believed to prefer breaking bonds along the [111] direction into the six-atom ring, which then reconstructs into a more compact and symmetric form, possibly a distorted trigonal bipyramid. The geometries of clusters with seven atoms or more are found by adding atoms to the six-atom configuration until a new, relatively more compact cluster of the reconstructed ten-atom cage is achieved. By construction, the six- and ten-atom clusters are more compact, and the dominant occurrence of six-atom fragments from larger clusters is a logical consequence of the  $6+N$  ( $N=1-3$ ) structure. Although this simple model of BFB is qualitatively consistent with the experimental results, it is not unique, nor are the actual structures and cohesive energies of the clusters known.

Recent detailed calculations by Raghavachari and Logovinsky<sup>15</sup> (RL) and by Tománek and Schlüter<sup>16</sup> (TS) enumerating the ground-state geometries of silicon clusters have found close-packed structures with significantly lower energy than the corresponding microcrystals, consistent with the experimental data. Both calculations employed a quantum-chemical approach, seeking the solution to the Schrödinger equation whose Hamiltonian included ion-ion, ion-electron, and electron-electron interactions. A complete solution to the Schrödinger equation

for finite temperatures is certainly a formidable task and not available for even small silicon clusters. Present methods attempt only to determine approximate ground-state geometries and electronic configurations.

The results of RL were based on the all-electron molecular orbital technique.<sup>21</sup> Several likely geometries and electron configurations were considered for each silicon cluster  $N=2-6$ . Equilibrium structures were determined by minimizing the total energy for both the neutral and ionized clusters. To avoid the possibility of metastable configurations, the harmonic vibrational frequencies of each cluster were calculated and found to be positive. Charged clusters were found to have nearly the same structure as the parent neutral clusters. Detailed analysis of charge distributions indicated that the least bonded atom usually carried a positive charge. A few configurations based on the results of  $\text{Si}_{2-6}$  were considered for  $\text{Si}_7$  and  $\text{Si}_{10}$ . The most stable zero-temperature structures found for  $\text{Si}_{3-7}$  were the isosceles triangle, planar rhombus, "flattened" trigonal bipyramid, edge-capped trigonal bipyramid, and tricapped tetrahedron, respectively. Of the geometries considered, a tetracapped octahedron had the lowest total energy for  $\text{Si}_{10}$ . The authors note that each cluster  $\text{Si}_N$  ( $N=3-7$ ) can be constructed by adding either an edge- or face-capped atom to the  $\text{Si}_{N-1}$  structure, with small clusters preferring edge-capping. Since the tricapped tetrahedron  $\text{Si}_7$  can be viewed as a distorted face-capped octahedron and  $\text{Si}_{10}$  is a tetracapped octahedron, it is natural to imagine  $\text{Si}_8$  and  $\text{Si}_9$  as bicapped and tricapped octahedrons, respectively. Again one has a model for Si microclusters, where  $\text{Si}_6$  fragments occur naturally from a  $6+N$  structure. The fragmentation energy (the smallest energy necessary to break the ground-state structure of each cluster) was also calculated and found to be relatively large for  $\text{Si}_4$  and  $\text{Si}_6$ . The existence of magic numbers ( $N=4,6$ ) was explained by the relatively low ground-state energies and the high fragmentation energies of  $\text{Si}_4$  and  $\text{Si}_6$ .

Tománek and Schlüter<sup>16</sup> actually perform two separate calculations to determine the ground-state energy of  $\text{Si}_N$  ( $N=2-11$ ) microclusters. The results of a tight-binding (TB) approach were used as input for a local-density approximation (LDA) in the density-functional theory (DFT).<sup>22-24</sup> The total energy was given by an empirical tight-binding Hamiltonian as developed by Chadi.<sup>25</sup> Starting with a number of different bonding configurations (10 to 20) Tománek and Schlüter found equilibrium structures through minimization of the total TB energy. The resulting stable or metastable configurations (2 to 3) were then investigated in more detail using the self-consistent local-density-functional approach with a Hamann-Schlüter-Chaing-type<sup>16</sup> pseudopotential to calculate total energies. Neutral, positively, or negatively charged clusters were found to have similar structures. The two methods agree quite well, with only small quantitative differences in bond lengths and cohesive energies. Ground-state structures for  $\text{Si}_{3-6}$  are the triangle, flat rhombus, "squashed" trigonal bipyramid, and the tetragonal bipyramid, respectively. The "squashed" (TS) and "flattened" (RL) trigonal bipyramids for  $\text{Si}_5$  are indicative of tightly bound caps relative to the pyramid's base.

Larger clusters ( $\text{Si}_7-\text{Si}_{14}$ ) in the TS model are constructed by adding face-capped atoms to the octahedron, which is then relaxed to give the final stable structure.  $\text{Si}_{14}$  is particularly symmetric, with every face of the octahedron capped. All configurations have lower energy than their corresponding microcrystalline fragments. The authors indicate that the TB calculation gives relatively stable configurations for  $N=4,6,10$ , while only  $N=6,10$  are found to be particularly stable from LDA.

Saito, Ohnishi, and Sugano<sup>19</sup> have constructed a model potential for calculating binding energies of silicon microclusters  $\text{Si}_N$ ,  $N=2-20$ . Each Si atom is considered to have four attractive centers located on the corners of a regular tetrahedron. The anisotropy lies in the attractive part of the interaction and depends on the relative orientation of the atoms. Yukawa's potential is adopted for the repulsive term. For the  $\text{Si}_2$  dimer, "corner-sharing" atoms with mirror symmetry about the bond connecting the two corners produces the most stable configuration, while "face-sharing" atoms are the most repulsive. Lowest-energy configurations were determined by minimizing the total energy with respect to rotations and translations of the atoms. Two stable configurations were found for each cluster  $N \geq 6$ . One set was found to contain only six-membered rings with structures similar to subunits of the diamond lattice. The remaining set, considered to be amorphous, contained mainly four- and five-membered rings with energies generally lower than the corresponding crystal fragments. Based on relatively high binding energies per atom, the authors claim the magic numbers for (i) the microcrystalline series are  $N=6, 10, 14$ , and 18, (ii) the amorphous series are  $N=5, 10, 12, 16, 18$ , and 20. The triangle, flattened tetrahedron, and regular pentagon are the most stable configurations for  $N=3, 4$ , and 5, respectively.  $\text{Si}_6$  is formed from  $\text{Si}_5$  by the addition of a corner-shared atom, while edge-shared atoms added to  $\text{Si}_6$ , forming four- and five-membered rings, were found to be the most stable structures for  $N > 6$ .

The above four approaches restrict calculations to zero-temperature ground-state configurations and impose strict limitations on the sampling of points in the  $3N$ -dimensional configuration space. This is not surprising, considering the enormous complexity of this few-body, finite-temperature problem. At best, the global ground-state configuration could be determined for small clusters by well-chosen initial positions. It may then be possible to determine the magic numbers and the most likely fragmentation channels from the ground-state binding energies and structures. However, the relationship between the lowest-energy zero-temperature configuration and the energetics of finite-temperature ( $T \sim 2000$  K) microclusters is not obvious. Since the dissociation of Si clusters in the photofragmentation experiment occurs at temperatures the order of the melting temperature, a first-principles finite-temperature calculation is needed that allows determination of all possible structures, their corresponding binding energies and the nature of fragmentation. There are two methods that may provide the means to perform such a calculation in the future: the Green's-function Monte Carlo (GFMC) technique<sup>26-28</sup> and the method of dynamical simulated annealing.<sup>29,30</sup> An

*ab initio* calculation using either of these two methods still presents considerable difficulty.

A very informative study can be performed by accepting a phenomenological potential for input in a detailed molecular-dynamics (MD) simulation.<sup>31</sup> In this way, one can explore the  $3N$ -dimensional configuration space in great detail, determining the underlying mechanically stable structures visited by the system in the equilibrium state at high temperatures and their corresponding binding energies and fragmentation spectra for microclusters ( $N=2-200$ ) within a reasonable computation time. In this paper, the results of such a MD simulation are presented for  $\text{Si}_N$  ( $N=2-14$ ), utilizing the Stillinger and Weber<sup>32</sup> three-body interaction potential. The presence of magic numbers, unusually stable finite-temperature  $N$ -atom clusters, is found by determining the fragmentation temperature ( $T_f$ ), the temperature at which the clusters fragment. Our results indicate that the magic numbers in the fragmentation spectra are determined by the topology and energetics of high-energy bound structures rather than by the structure and ground-state energies at zero temperature.

Section II presents the interaction potential and general techniques employed. The Stillinger-Weber phenomenological potential is discussed in Sec. II A, followed by a brief summary of the molecular-dynamics technique in Sec. II B. The steepest-descent quench, an important technique for enumerating the underlying mechanically stable structures of the finite-temperature clusters, is presented in Sec. II C. Section III contains a detailed amount of the MD simulation, describing how the global ground-state structures, the most probable structure underlying the finite-temperature cluster, and the fragmentation spectra were obtained. Section IV presents results for the ground-state structures for  $\text{Si}_{2-14}$  and a comparison of RL and TS. Section V contains results for finite-temperature clusters. Section V A presents energy versus temperature curves, discusses their interesting features, and describes how the internal energy depends upon temperature. The hidden structures underlying the finite-temperature clusters are discussed in Sec. V B. The evidence for the existence of unusually stable microclusters  $\text{Si}_{4,6,10}$  (magic numbers) is discussed in Sec. VI.

## II. INTERACTION POTENTIAL, MOLECULAR-DYNAMICS TECHNIQUE, AND METHOD OF STEEPEST DESCENTS

### A. The Stillinger-Weber silicon potential

Considering two- and three-body interactions, Stillinger and Weber<sup>32</sup> (SW) recently devised a phenomenological potential for silicon. The three-body contribution always increases the total potential energy when the angle formed by a central atom and two of its covalently bonded neighbors differs from the perfect tetrahedral angle. All energies resulting from the present work are expressed in units of  $\epsilon$ , the magnitude of the minimum in the two-body potential, and all lengths are expressed in units of  $\sigma$ . Values of  $\epsilon$  (50 kcal=2.17 eV) and  $\sigma$  (2.0951 Å) were chosen to give the correct atomization energy and density of crystal-

line silicon at zero temperature and pressure. In reduced units a temperature ( $T^*$ ) of 0.1 corresponds to 2500 K.

The two-body contribution to the SW potential has the following functional form:

$$V_2(\mathbf{r}_i, \mathbf{r}_j) = V_2(r_{ij}) \\ = \sum_{i < j} A (B r_{ij}^{-p} - r_{ij}^{-q}) \exp[(r_{ij} - a)^{-1}], \quad (2.1)$$

and the three-body term is taken to be

$$V_3(\mathbf{r}_i, \mathbf{r}_j, \mathbf{r}_k) = h(r_{ji}, r_{ki}) + h(r_{kj}, r_{ij}) + h(r_{ik}, r_{jk}), \quad (2.2)$$

where

$$h(r_{ji}, r_{ki}) = \sum_{i < j < k} \lambda \exp\{\gamma[(r_{ji} - a)^{-1} + (r_{ki} - a)^{-1}]\} \\ \times (\cos\theta_{jik} + 1/3)^2. \quad (2.3)$$

We have used the notation  $r_{ij} = |\mathbf{r}_i - \mathbf{r}_j|$  and  $\theta_{jik}$  as the angle subtended by  $\mathbf{r}_{ji}$  and  $\mathbf{r}_{ki}$  with the vertex at  $i$ . The three-body contribution obviously becomes zero at the perfect tetrahedral angle  $\theta_t$  ( $\cos\theta_t = -\frac{1}{3}$ ) and is positive otherwise.

This functional form was chosen so that the potential and its derivatives approach zero continuously as the distance  $r$  nears the cutoff  $a$  and is set to zero for  $r$  greater than or equal to  $a$ . The parameters in this model potential, Eqs. (2.1)–(2.3), were determined from the cohesive energy of the diamond lattice, the melting temperature, and the local structure of molten silicon. The parameter set chosen by SW gives the diamond lattice as the most stable structure at low pressure and sc, bcc, and fcc lattices with slightly higher lattice energies. When compared with the diamond lattice, the sc, bcc, and fcc lattices have additional two, four- and eight two-body bonds, respectively, which tend to increase the total binding energy, while the deviations from perfect tetrahedral angles decrease the binding energy. These two competing effects, additional bonds, and deviations from tetrahedral angles, have the net result of decreasing the total binding energy relative to the perfect diamond configuration. The melting temperature and liquid structure factor resulting from the parameter set compared favorably with experimental results. The values of the seven parameters  $A$ ,  $B$ ,  $a$ ,  $p$ ,  $q$ ,  $\lambda$ , and  $\gamma$  for the SW potential are given below:

$$A = 7.049\,556\,277, \quad B = 0.602\,224\,558\,4, \\ a = 1.8, \quad p = 4, \quad q = 0, \\ \lambda = 21.0, \quad \gamma = 1.20.$$

The range of interaction ( $a = 3.77$  Å) is just short of the second-nearest-neighbor distance (3.83 Å) in the diamond crystal. Bulk properties, such as cohesive energy for the diamond lattice (4.34 eV/atom), the thermodynamic melting temperature ( $T_m = 2000$  K), and the nearest-neighbor distance (2.35 Å) determined from this potential are in good agreement with the experimental values of 4.63 eV/atom, 1688 K, and 2.35 Å, respectively.

### B. The molecular-dynamics technique

Molecular-dynamics simulation allows calculation of the static and dynamic properties of a system for a given interaction potential. The particle trajectories in real space are found by integrating Newton's equation of motion. In this way, the microscopic configurations as well as the collective dynamics of a large number of particles, typically  $N=100-5000$ , can be thoroughly investigated. The present work employed Beeman's algorithm<sup>33</sup> to integrate Newton's equations of motion,

$$x(t+\Delta t)=x(t)+v(t)\Delta t+[4a(t)-a(t-\Delta t)]\Delta t^2/6 \quad (2.4)$$

and

$$v(t+\Delta t)=v(t)+[2a(t+\Delta t)+5a(t)-a(t-\Delta t)]\Delta t/6. \quad (2.5)$$

Initial positions  $x(t=0)$  and velocities  $v(t=0)$  were chosen and the acceleration  $a(t)$  was determined from the SW force. After the initial conditions were chosen, the system was well thermalized at a given value of the internal energy. The initial conditions had no effect on the equilibrium properties. A time step ( $\Delta t$ ) of  $3.8 \times 10^{-16}$  sec was used, resulting in energy conservation to five significant digits. Various bonding geometries, including the lowest-energy configurations of RL and TS, were considered as initial conditions for each cluster, although final results were independent of the initial geometry. Microcrystalline fragments were found to have the lowest binding energies and were unsuitable starting configurations for large clusters ( $N > 8$ ). To start the MD run, each particle in the cluster was given both a small random displacement and velocity ensuring that both total linear and angular momenta of the cluster were initially set to zero. Subsequent scalings of the velocities to raise or lower the cluster's energy did not impart any linear or angular momentum to the system. All calculations were performed on the Ridge 32/130.

### C. The steepest-descent quench (SDQ)

The potential  $V(\mathbf{R})$  ( $\mathbf{R}=\{\mathbf{r}_1, \mathbf{r}_2, \dots, \mathbf{r}_N\}$ ) of an  $N$ -particle system defines a surface in the  $3N$ -dimensional configuration space. This surface may have many different minima identified with different stable or metastable structures. Such a collection of minima for bulk silicon would include all the various amorphous packings and the global minimum of the crystalline geometry. The time evolution of a finite-temperature cluster is represented by its trajectory on the constant-energy hypersurface in the  $6N$ -dimensional phase space. The projection of this trajectory on the  $3N$ -dimensional configuration space will pass in the neighborhood of all accessible potential-energy minima corresponding to allowed structures. One obvious advantage of MD simulations is the exact determination of most, if not all, mechanically stable configurations. The assignment of these finite-temperature structures to the underlying mechanically stable structures requires the partitioning of the potential-energy surface. Every point

in this configuration space must be uniquely identified with a local potential minimum. In this way, the instantaneous positions of the finite-temperature system can be considered as composed of vibrational (possibly anharmonic) displacements from the equilibrium positions of a local minimum. This is a mathematically well-defined problem that can be solved through the steepest-descent quench.<sup>34</sup> The SDQ assigns each point on the potential-energy surface in configuration space to the first potential minimum encountered when descending from that point along the steepest available path. The determination of the local minimum is performed by solving the steepest-descent equation

$$\frac{\partial \mathbf{R}}{\partial s} = -\nabla_{\mathbf{R}} V(\mathbf{R}) \quad (2.6)$$

in the limit  $s \rightarrow \infty$ . The actual solution to this equation was found through the conjugate-gradient method, an efficient numerical solution for a function of many variables.

At very low energies, the particles oscillate about the equilibrium positions of their initial  $T=0$  configuration, and transitions between states prohibited by the potential barriers. Mapping instantaneous positions of such a system to the local equilibrium positions will always yield one configuration, a mechanically stable structure with ( $\mathbf{F}_i=0$ ) and ( $\mathbf{v}_i=0$ ). For higher energies, the potential barriers are overcome and the system is allowed to change structure. If that were to occur, the lowest-energy route between neighboring minima would pass over a potential barrier characterized by a saddle point lying on the line separating the two neighboring regions of the partitioned surface. In this case, mapping of the instantaneous positions will result in two or more distinct mechanically stable structures. As the system is heated, more and more structures become accessible until dissociation is permitted. The investigation of these structures is one of the principle objectives of the present work.

## III. METHOD OF CALCULATION

An exhaustive search was carried out to (i) enumerate all accessible mechanically stable configurations and the relative probabilities of occupying any particular configuration at given finite temperatures, (ii) find the highest energy ( $E_f$ ) and temperature ( $T_f$ ) at which the system would remain bound, and (iii) determine the distribution of fragmentation channels for each cluster ( $N=3-14$ ). Ideally, the fragmentation energy  $E_f$  should be defined as the lowest energy at which a system fragments on a macroscopic time scale. However, this is an unrealistic requirement for the present calculation, so we have defined the fragmentation energy to be the highest energy before the first fragmentation event at which the system remains bound for 25 000 MD steps.

Initially, each cluster was monotonically heated until very high energies were reached, generating a large number of systems (10-20) of various energies to be used later for determination of the fragmentation energy. At each energy the system was thermalized for 1000 time steps.

Subsequently, the temperature was defined through the average kinetic energy over many thousands of time steps. The total energy of a cluster was increased until the system fragmented. The mechanically stable structures and corresponding binding energies underlying the finite-temperature clusters were determined from SDQ mappings of the configuration-space trajectory to the local minima, as shown schematically in Fig. 1. In this way, approximately 1000 mechanically stable configurations were recorded for each cluster, although only a small subset was actually unique structures. The systems which did not fragment had been well “thermalized” (11000 MD steps) and served as seeds for subsequent determination of the most likely fragmentation channels. These systems were heated (or cooled, for superheated systems) once every 11000 steps until fragmentation occurred. Between 20 and 30 fragmentations were observed for each cluster  $\text{Si}_N$  ( $N=3-14$ ). The fragmentation energy as defined above was determined to within  $0.01\epsilon$  ( $0.02$  eV/atom) by making a series of simulations of 25000 MD steps in the energy range of interest.

To determine the relative probability of visiting certain geometries, all clusters were started from their zero-temperature ground-state configuration and monotonically heated. Through this procedure, one finds only those structures accessible from the ground state. Four systems were generated by stepwise heating the lowest-energy structure until 25%, 50%, 75%, and 95% of the energy required for fragmentation had been added. The energies of the resulting four systems are referred to below as  $0.25E_f$ ,  $0.5E_f$ ,  $0.75E_f$ , and  $0.95E_f$ , respectively. The relative probabilities of visiting particular configurations

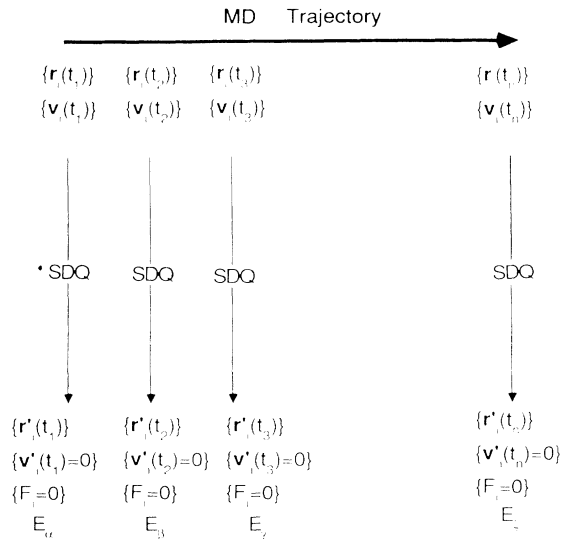


FIG. 1. Schematic representation of the steepest-descent quench (SDQ) performed in parallel with the molecular-dynamics (MD) simulation. MD generates positions  $\{r_i\}$  and velocities  $\{v_i\}$  at each time step through integration of Newton's equation of motion. The SDQ maps the instantaneous positions to the local minimum  $E_\alpha$  where the force  $\{F_i\}$  on each particle vanishes and the velocities are zero. This mapping does not in any way affect the continuation of the MD trajectory.

were determined at these four energies by frequent mappings to the local potential minima during a 5000-step, constant-energy MD run.

#### IV. GROUND-STATE STRUCTURES

The lowest-energy structures for each cluster  $\text{Si}_{3-14}$  were determined from approximately 1000 mapped potential minima performed in the first part of this work. Steepest-descent mappings were also carried out parallel with a MD run for  $\text{Si}_2$ . As expected for this model potential, the distance separating the two atoms in the dimer is exactly the nearest-neighbor distance in crystalline silicon. The ground-state configurations of  $\text{Si}_3$ ,  $\text{Si}_4$ , and  $\text{Si}_5$  have the following symmetrical and planar geometries: the equilateral triangle [Fig. 2(a)], the square [Fig. 3(a)], and the regular pentagon [Fig. 4(a)], respectively. It should be noted that the isosceles triangle [Fig. 2(b)], consisting of only two bonds forming a perfect tetrahedral angle, is only slightly higher in energy than the ground-state structure of  $\text{Si}_3$ . The loss is the two-body binding energy of this metastable state with respect to the lowest-energy configuration due to the decrease in the number of bonds is offset by the three-body interaction. A more complete discussion of the high-energy structures for  $\text{Si}_{3-14}$  is given in the section on hidden structures (Sec. V B). It is not surprising the pentagon has the lowest energy for  $\text{Si}_5$  since the angle between adjacent bonds ( $108^\circ$ ) is only  $1.5^\circ$  smaller than the perfect tetrahedral angle. The squashed trigonal bipyramid [Fig. 4(b)], whose energy is higher than the ground state of the pentagon by less than 1%, was also commonly found during steepest-descent quenches from intermediate temperatures. The structure of  $\text{Si}_N$  ( $N=3,4,5$ ) can be understood in terms of relaxing the edge-capped  $\text{Si}_{N-1}$  structure.

The triangle is the basic subunit in the formation of the  $\text{Si}_6$  and  $\text{Si}_7$  ground states. The ground-state structure of  $\text{Si}_6$  is the first to have three-dimensional geometry with all atoms threefold coordinated. The symmetrical stacking of two equilateral triangles, similar to a wedge, form the  $\text{Si}_6$  structure [Fig. 5(a)], while the  $\text{Si}_7$  ground-state configurations [Fig. 6(a)] can be thought of as capping each of the three edges on the base of the trigonal pyramid. The  $\text{Si}_7$  structure containing one equilateral, and six nearly equilateral, isosceles triangles may be achieved from the reconstruction of an edge-capped  $\text{Si}_6$  ground-state configuration.

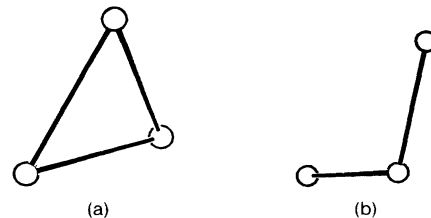


FIG. 2.  $\text{Si}_3$  structures: (a) ground-state structure, equilateral triangle,  $E = -0.6828\epsilon$ ; (b) isosceles triangle with the only two bonds forming a perfect tetrahedral angle ( $\text{Si}_3$  chain),  $E = -0.6667\epsilon$ .

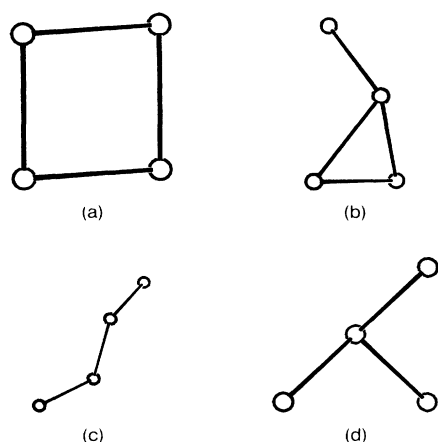


FIG. 3.  $\text{Si}_4$  structures: (a) ground-state structure, square,  $E = -0.9387\epsilon$ ; (b) corner-capped equilateral triangle,  $E = -0.7621\epsilon$ ; (c) and (d) lowest-binding-energy configurations, degenerate in energy with three bonds and perfect tetrahedral angles,  $E = -0.7500\epsilon$ .

One can form the symmetric ground-state geometry of  $\text{Si}_8$ , a perfect cube [Fig. 7(a)], by either reconstructing a face-capped  $\text{Si}_7$  structure or by attaching a  $\text{Si}_2$  dimer to a square face of the  $\text{Si}_6$  wedge. The addition of one atom to the edge of the  $\text{Si}_8$  cube forms the lowest-energy structure for  $\text{Si}_9$  [Fig. 8(a)]. Allowing this structure to relax breaks

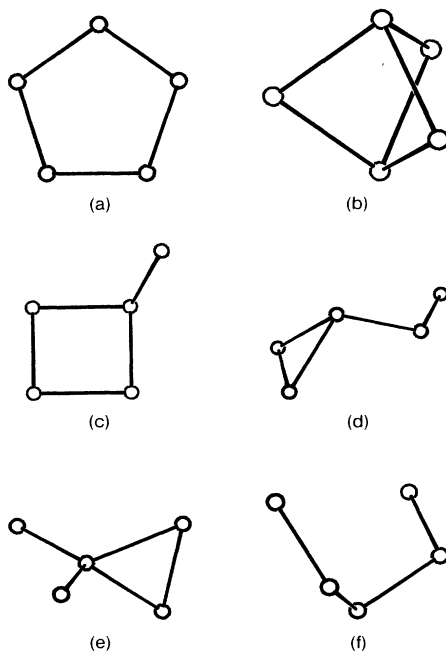


FIG. 4.  $\text{Si}_5$  structures: (a) ground-state structure, pentagon,  $E = -0.9996\epsilon$ ; shown in order of decreasing binding energy, other structures are (b) trigonal bipyramid,  $E = -0.9899\epsilon$ ; (c) corner-capped square,  $E = -0.9509\epsilon$ ; (d) two-atom chain corner-capped to an equilateral triangle,  $E = -0.8097\epsilon$ ; (e) reconstructed tetrahedron,  $E = -0.8029\epsilon$ ; (f) fragment of the crystalline six-atom chair ring ( $\text{Si}_5$  chain),  $E = -0.8000\epsilon$ .

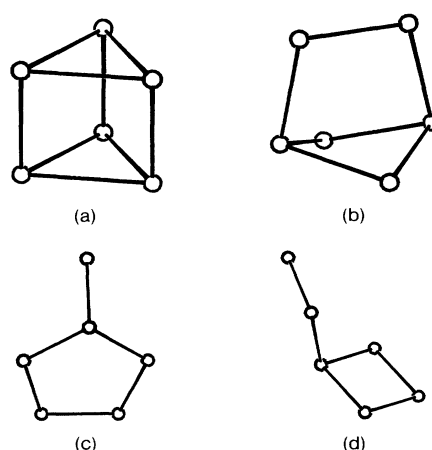


FIG. 5.  $\text{Si}_6$  structures: (a) ground-state geometry can be formed by symmetrically stacking two equilateral triangles,  $E = -1.0906\epsilon$ ; (b) reconstructed face-capped pentagon,  $E = -1.0867\epsilon$ ; (c) corner-capped pentagon,  $E = -0.9997\epsilon$ ; (d) two-atom chain corner-capped to a square,  $E = -0.9591\epsilon$ .

the edge-capped bond, forming two identical, nearly perpendicular, nonplanar pentagons. The ground-state geometry for  $\text{Si}_5$  may be used to obtain  $\text{Si}_{10}$  in the same way the ground-state structures for  $\text{Si}_N$  ( $N=2,3,4$ ) can be used to obtain those of  $\text{Si}_{2N}$  with the lowest-energy configuration for  $\text{Si}_{10}$  made of two symmetrically stacked pentagons [Fig. 9(a)]. This structure may also be formed by face-capping the  $\text{Si}_9$  ground-state configuration or by adding a dimer parallel to one face of the  $\text{Si}_8$  cube.

Reconstruction of an atom capped to a pentagon face on the  $\text{Si}_{10}$  ground-state structure results in the lowest-energy configuration for  $\text{Si}_{11}$  [Fig. 10(a)]. The ground-state structure for  $\text{Si}_{11}$  is the smallest to contain a fourfold-coordinated atom. The symmetrical ground-state figure for  $\text{Si}_{12}$  [Fig. 11(a)] can perhaps be more easily described by the addition of a  $\text{Si}_2$  dimer to a square face

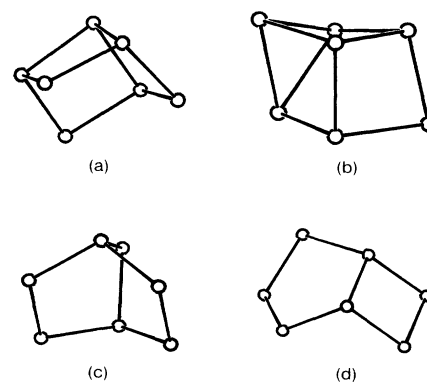


FIG. 6.  $\text{Si}_7$  structures: (a) ground-state structure,  $E = -1.1788\epsilon$ ; (b) most commonly found low-energy structure,  $E = -1.1778\epsilon$ ; (c) dimer face-capped to a pentagon,  $E = -1.1128\epsilon$ ; (d) square edge-sharing with a pentagon,  $E = -1.1075\epsilon$ .

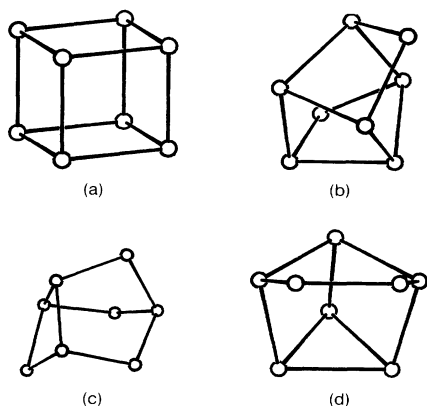


FIG. 7.  $\text{Si}_8$  structures: (a) ground-state structure, cube,  $E = -1.3222\epsilon$ ; shown in order of decreasing binding energy, (b)  $E = -1.2364\epsilon$ , (c)  $E = -1.2020\epsilon$ , (d)  $E = -1.1903\epsilon$ . These three structures account for over 50% of the underlying structure at energies near  $E_f$ .

of the  $\text{Si}_{10}$  ground state, but can also be obtained by face-capping the  $\text{Si}_{11}$  ground state so that one of the tetrahedral bonds is broken. The ground-state geometry for  $\text{Si}_{12}$  has four identical pentagons bound in stacked pairs orientated perpendicular to one another and pointing in opposite directions. Similar to  $\text{Si}_{11}$ , the ground-state structure of  $\text{Si}_{13}$  [Fig. 12(a)], contains one fourfold-coordinated atom. The configuration is best described by the edge sharing of four identical pentagons to create a four-sided cone, with the small end forming a square and the open end capped by an atom connected to each of the four protruding points. The  $\text{Si}_{14}$  ground-state geometry [Fig. 13(a)], similar to all even numbered clusters, is very symmetrical, consisting of six identical pentagons and

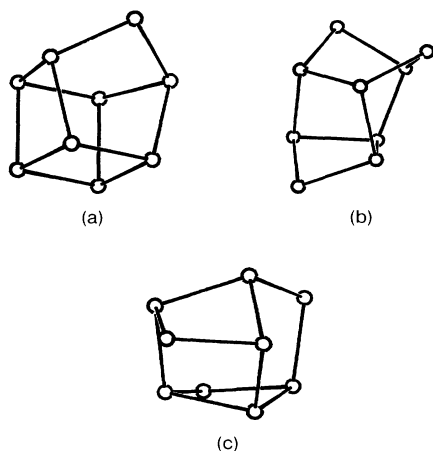


FIG. 8.  $\text{Si}_9$  structures: (a) ground-state geometry can be constructed from an edge-capped cube,  $E = -1.3271\epsilon$ ; the two most common configurations, besides the ground state, that result from the SDQ at energies near  $E_f$  (b)  $E = -1.2612\epsilon$  and (c)  $E = -1.2455\epsilon$ .

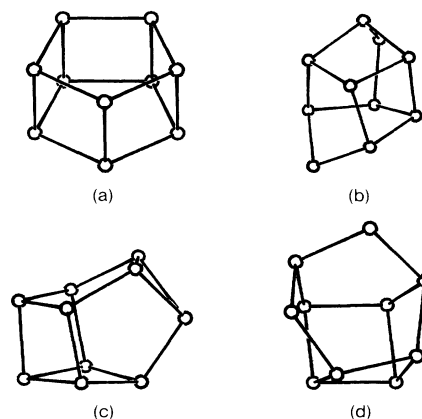


FIG. 9.  $\text{Si}_{10}$  structures: (a) ground-state geometry can be formed by symmetrically stacking two regular pentagons,  $E = -1.3797\epsilon$ ; most commonly visited structures near  $E_f$  (b)  $E = -1.3309\epsilon$ , (c)  $E = -1.328\epsilon$ , and (d)  $E = -1.3178\epsilon$ .

three perfect squares, with all atoms lying on the surface having only three bonds.

Several features appear common to all  $\text{Si}_N$  ( $N=3-14$ ) microclusters interacting through the SW three-body potential. First, one observes the existence of three basic “building blocks” (triangle, square, and pentagon) in the ground-state energy structures for each cluster  $\text{Si}_{3-14}$ . These not only form the lowest-energy configurations for  $\text{Si}_3$ ,  $\text{Si}_4$ , and  $\text{Si}_5$  but one also obtains the ground-state configurations of  $\text{Si}_6$ ,  $\text{Si}_8$ , and  $\text{Si}_{10}$  by trivially stacking these three planar figures. All metastable configurations for large clusters are formed by three-, four-, and five-membered rings which are the distorted ground-state configurations for  $\text{Si}_3$ ,  $\text{Si}_4$ , and  $\text{Si}_5$ . The concept of basic building blocks underlying complex structures has been

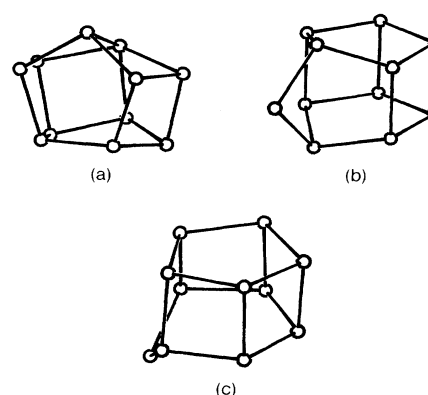


FIG. 10.  $\text{Si}_{11}$  structures: (a) ground-state structure, smallest structure to contain a fourfold-coordinated atom,  $E = -1.3829\epsilon$ ; (b) frequently found structure of nearly the same energy as the ground state,  $E = -1.3789\epsilon$ ; (c) dominant underlying structure near  $E_f$ ,  $E = -1.3600$ . Note all three configurations can be easily obtained by adding either an atom to the face or edge of the  $\text{Si}_{10}$  ground-state structure.

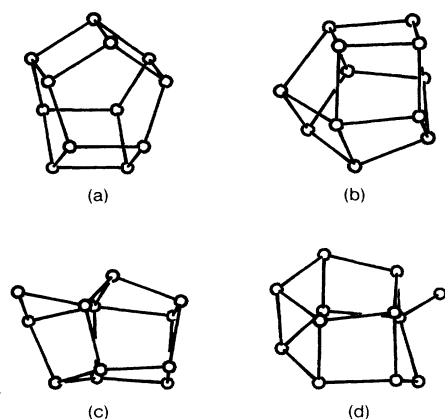


FIG. 11.  $\text{Si}_{12}$  structure: (a) ground-state configuration has four identical pentagons and four squares,  $E = -1.4178\epsilon$ ; most frequently found structures near  $E_f$  (b)  $E = -1.3968\epsilon$ , (c)  $E = -1.3730\epsilon$ , and (d)  $E = -1.3290\epsilon$ .

previously used by Chadi<sup>35</sup> to construct new crystalline forms for Si and Ge.

A comparison of the present results with those of RL and TS is presented in Fig. 14 for  $\text{Si}_{2-6}$ . Our calculated binding energies are consistently lower than the quantum-chemical calculations due to the SW potential's inability to correctly evaluate the interaction energy between underbonded atoms. Nonetheless, the lowest-energy configurations determined by the two previous calculations<sup>15,16</sup> do routinely appear in the MD results, with the additional possibility of lower-energy structures for  $\text{Si}_5$  and  $\text{Si}_6$ . The ground-state configurations for  $\text{Si}_{7-12}$  determined from the present MD simulation can be constructed by the addition of atoms to the lowest-energy  $\text{Si}_6$  structure similar to the previous work. Consequently, this model potential could also predict the natural occurrence

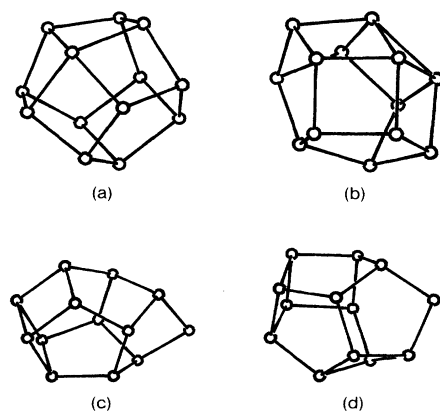


FIG. 12.  $\text{Si}_{13}$  structures: (a) ground-state contains one fourfold-coordinated atom,  $E = -1.4234\epsilon$ ; two commonly found low-energy structures are shown in (b), containing four fourfold-coordinated atoms,  $E = -1.4138\epsilon$  and (c), containing only threefold coordinated atoms,  $E = -1.4136\epsilon$ ; (d) an example of a low-binding energy, bound structure,  $E = -1.3988\epsilon$ .

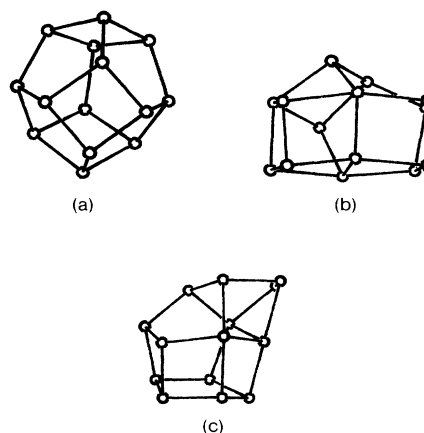


FIG. 13.  $\text{Si}_{14}$  structures: (a) ground-state structure consists of six identical pentagons and three squares,  $E = -1.4455\epsilon$ ; two examples of the other 155 possible configurations accessible to this 14-atom cluster at high temperatures, (b)  $E = -1.4069\epsilon$  and (c)  $E = -1.3960\epsilon$ .

of  $\text{Si}_6$  fragments from the  $6 + N$  ( $N = 1-8$ ) structure if dissociation occurred from the ground state. The plot of ground-state energy per atom ( $E_0$ ) versus number ( $N$ ) in Fig. 15(a) does not show any indication of the existence of the magic numbers ( $N = 4, 6, 10$ ) that appear in the plots by RL [Fig. 15(b)] and TS [Figs. 15(c) and 15(d)]. In the calculations of RL and TS, a limited search of possible ground-state geometries resulted in relatively stable structures for  $\text{Si}_{4,6,10}$ . The unusually common occurrence of these clusters in the photofragmentation spectra of silicon was then explained by their particularly stable ground-state configurations. We have found structures topologically equivalent to the ground-state structures of RL and TS, although for  $\text{Si}_5$  and  $\text{Si}_6$  new structures of higher binding energies were also obtained. We believe that the existence of magic numbers ( $N = 4, 6, 10$ ) cannot be explained from a consideration of the ground-state energies [Fig. 15(a)], or zero-temperature structures. In the present work, even-numbered clusters have relatively stable ground-state structures due to their symmetrical forms, which tends to maximize the number of bonds while minimizing the three-body potential energy.  $\text{Si}_6$  is the only exception, due to the large contribution of the two equilateral triangles to the three-body energy.

Our calculated ground-state structures contain only four- and five-membered rings for large clusters ( $N = 8-14$ ), similar to the "amorphous" clusters of Saito *et al.*,<sup>19</sup> and are in excellent agreement with their small clusters  $\text{Si}_2$ ,  $\text{Si}_3$ , and  $\text{Si}_5$ . However, the large clusters determined by these authors have open structures containing many two-bonded atoms. These structures also appear in our results, but only when the system at high temperature is analyzed by SDQ to examine the underlying mechanically stable structures of higher energy.

In contrast to RL, TS, and Saito *et al.*, we are unable from the zero-temperature ground-state energies and structures to make any claims for the presence of magic numbers, even though our calculated structures for silicon



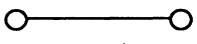
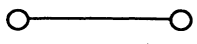
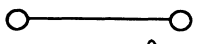
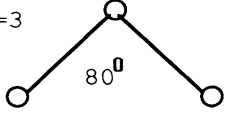
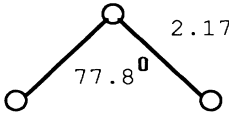
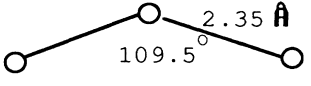
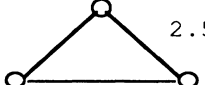
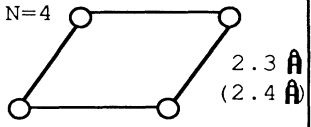
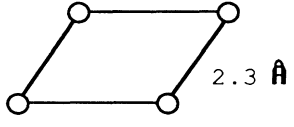
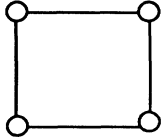
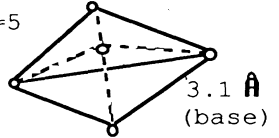
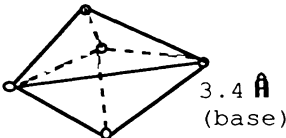
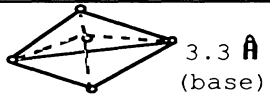
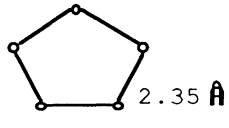
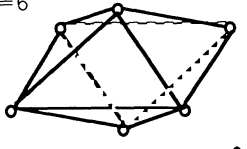
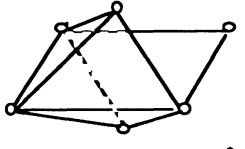
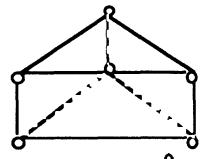
TS	RL	PRESENT
<p>N=2</p>  <p>2.27 Å</p> <p>E=1.54 eV</p>	 <p>2.23 Å</p> <p>E=1.57 eV</p>	 <p>2.25 Å</p> <p>E=1.08 eV</p>
<p>N=3</p>  <p>80°</p> <p>E=2.2 eV E=2.2 eV (LDA)</p>	 <p>77.8°</p> <p>2.17 Å</p> <p>E=2.57 eV</p>	 <p>109.5°</p> <p>2.35 Å</p> <p>E=1.44 eV</p>  <p>2.56 Å</p> <p>E=1.48 eV</p>
<p>N=4</p>  <p>2.3 Å (2.4 Å)</p> <p>E=3.1 eV E=2.8 (LDA)</p>	 <p>2.3 Å</p> <p>E=3.34 eV</p>	 <p>2.4 Å</p> <p>E=2.03 eV</p>
<p>N=5</p>  <p>3.1 Å (base)</p> <p>E=2.9 eV E=3.3 eV (LDA)</p>	 <p>3.4 Å (base)</p> <p>E=3.34 eV</p>	 <p>3.3 Å (base)</p> <p>E=2.15 eV</p>  <p>2.35 Å</p> <p>E=2.17 eV</p>
<p>N=6</p>  <p>2.6 Å</p> <p>E=3.5 eV</p>	 <p>2.32 Å</p> <p>E=3.65 eV</p>	 <p>2.35 Å</p> <p>E=2.36 eV</p>

FIG. 14. Comparison of ground-state structures and binding energies resulting from the present calculation with those determined from approximate solutions to the Schrödinger equation as carried out by Tománek and Schlüter (TS) and by Raghavachari and Logovinsky (RL).

microclusters are in accord with the previous work. The present static zero-temperature results indicate that all even-numbered clusters (particularly  $\text{Si}_8$ ) are relatively stable, with the exception of  $\text{Si}_6$ . The ground-state configurations for  $\text{Si}_N$  ( $N=7-14$ ) can be constructed from

$\text{Si}_{N-1}$  with  $\text{Si}_6$  as the basic subunit, but that is a weak argument for the mechanism of fragmentation and an insufficient explanation for the common occurrence of  $\text{Si}_6$  fragments, especially when fragmentation occurs at such high temperatures. The structures underlying the high-

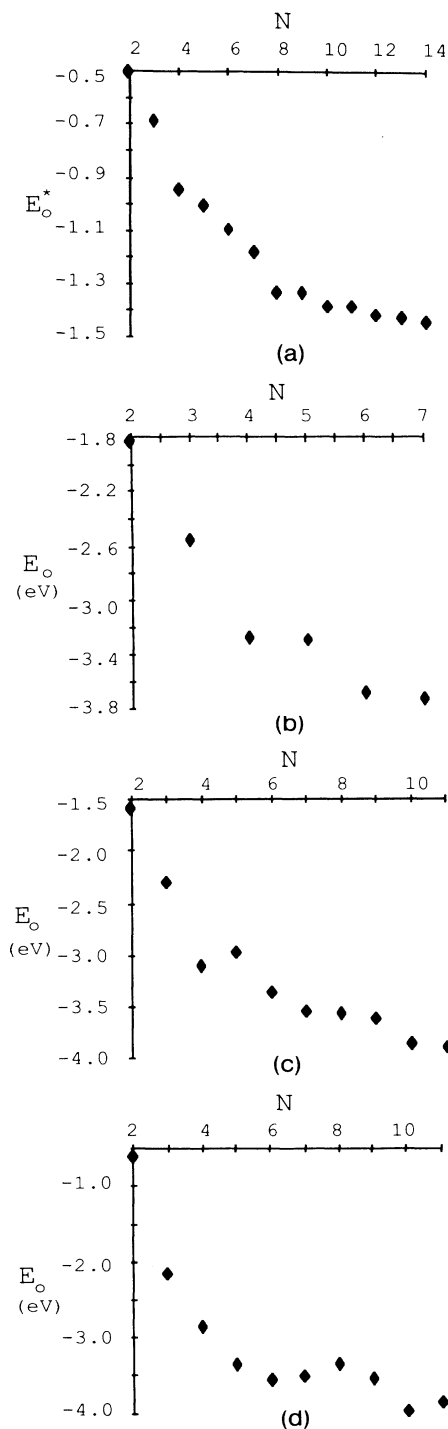


FIG. 15. Ground-state energy per atom ( $E_0$ ) vs number ( $N$ ) for (a) present results, in the reduced units of energy ( $\epsilon$ ); (b) Raghavachari and Logovinsky, Hartree-Fock calculation; (c) Tománek and Schlüter, tight-binding calculation; (d) Tománek and Schlüter, local-density approximation. The unusually common occurrence of  $\text{Si}_{4,6,10}$  in the photofragmentation spectra obtained by BFB is explained by RL and TS as due to the relative stability of their ground-state configurations. In the present calculation, the presence of magic numbers cannot be explained by ground-state energies or structures but only by the topology and energetics of finite-temperature clusters.

temperature cluster must play an important role in the determination of fragmentation spectra, and they can only be studied by investigating finite-temperature systems.

## V. CLUSTERS AT HIGH TEMPERATURES

### A. Temperature dependence of the total internal energy

The curves of total internal energy per atom ( $E$ ) versus temperature ( $T$ ) are given for each cluster  $\text{Si}_{3-14}$  in Fig. 16. It is apparent that there exist several small jumps similar to structural transformations, particularly for small clusters,  $\text{Si}_{3-6}$ . These steps are indicative of the change in the majority of underlying mechanically stable states from lower- to higher-energy structures, rather than of a single structural transition. An investigation of the clusters lacking this feature in the  $E$  versus  $T$  curve has shown them to possess a large number of accessible structures, with small differences in energies that span the range between low- and high-energy configurations. Since the transition from the lowest- to the highest-energy structures involves many intermediate configurations, the shift in the majority of underlying structures occurs smoothly and a sharp transition cannot be seen in  $E$  versus  $T$ . In some cases, many states are accessible but are grouped into subsets of structures of nearly equal energies with each group separated by relatively large energy differences, such that the transition between different subsets also appears as a small step in  $E$  versus  $T$ . As an example,  $\text{Si}_6$  has 16 different configurations, which can be grouped into three subsets of nearly equal binding energies, giving rise to two small jumps in  $E$  versus  $T$  [Fig. 16(d)]. The energy distribution of the underlying structures giving rise to these jumps is discussed below (Sec. VB).

### B. Hidden structures

Of the systems generated in the monotonic heating from the ground state of each cluster, four were chosen for a 5000-time-step MD run, with SDQ performed in parallel every fifth step (see Fig. 1) to enumerate the underlying mechanically stable configuration and to determine the relative probability of visiting each structure. Due to the large number of accessible configurations, only the ground-state structure and the most interesting higher-energy structures will be discussed for  $\text{Si}_{6-10}$ . The choice of which high-energy configurations were most pertinent was based on the relative number of visitations found by SDQ. The number of possible configurations given below for  $\text{Si}_{6-14}$  is for only those structures that appeared more than once in a given MD run where 1000 configurations were determined. Allowed structures which were not visited or seldom found are considered to be statistically unimportant. To simplify the following discussion, we will define "a chain of atoms" to be a bound cluster with all atoms except the two end atoms exactly twofold coordinated and all angles perfectly tetrahedral, with the three-body contribution to the total potential energy identically zero. In reduced units, the energy per atom of the  $\text{Si}_N$  chain is  $(N-1)/N$ , setting a

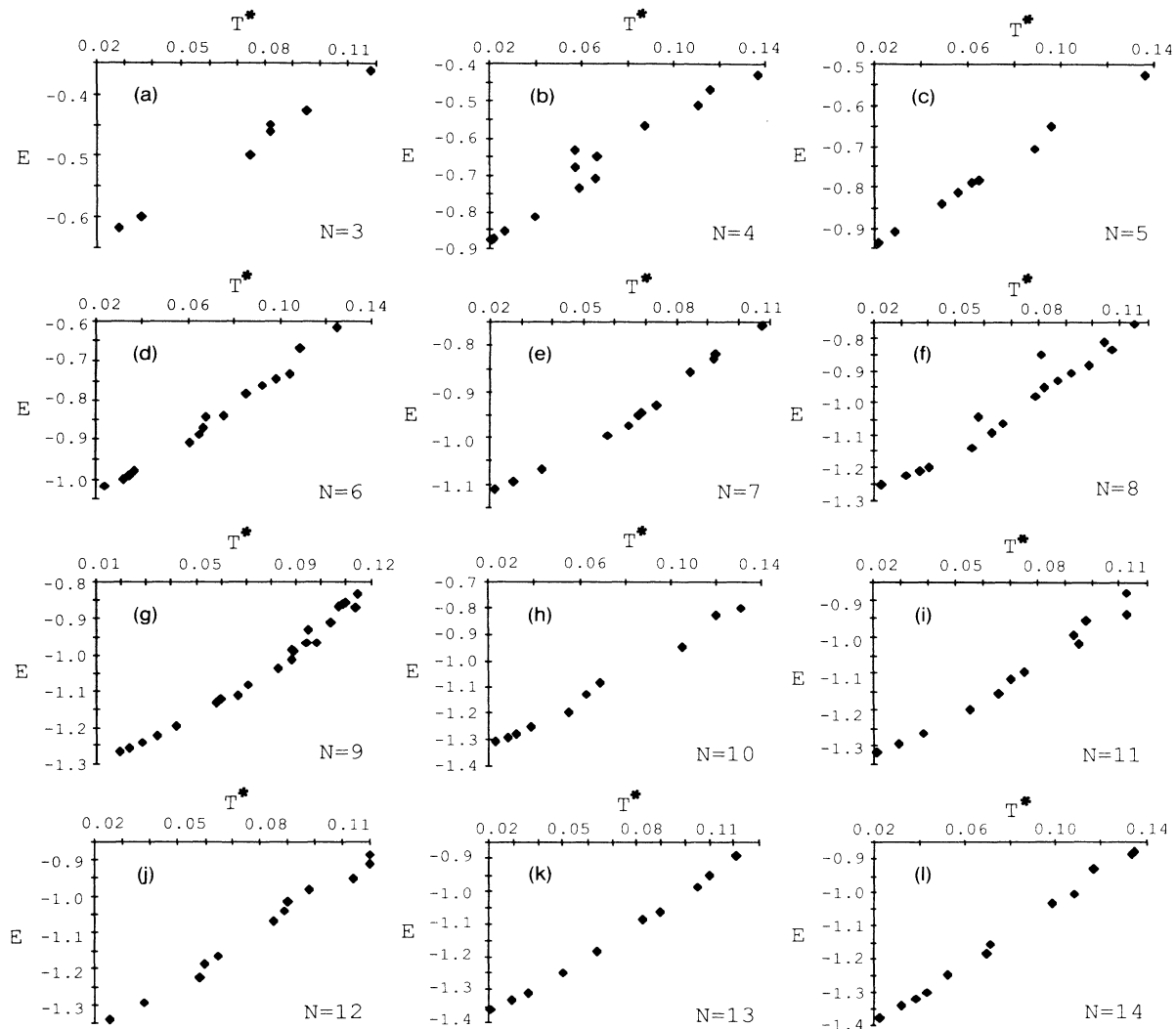


FIG. 16. Total internal energy per atom versus temperature curves are shown for  $\text{Si}_{3-14}$  in (a)–(l), respectively. Each cluster was started in its ground-state configuration and monotonically heated by multiplying the velocities by 1.1. After each scaling, the temperature was determined by averaging the kinetic energy over 11 000 MD steps. A reduce temperature ( $T^*$ ) of 0.1 corresponds to 2500 K.

lower limit on possible binding energies. There are several bound configurations for  $\text{Si}_N$  with  $(N-1)$  two-body bonds and only perfect tetrahedral angles, all degenerate in energy. The chain is the most stable of these structures since it has only two end atoms that are singly coordinated. These highest-energy structures are visited below  $E_f$  in  $\text{Si}_{3-6}$  and can be identified in superheated clusters up to  $\text{Si}_{11}$ . It should be noted that all of these high-energy structures can be considered fragments of the perfect diamond crystal.

$$N = 2$$

The dissociation energy for  $\text{Si}_2$  (the energy added to the zero-temperature cluster when fragmentation occurs) was determined to be  $\epsilon$  (2.17 eV/atom), the depth of the two-body potential well. This value is to be compared with

Honig's<sup>10</sup> experimentally determined value of  $1.5\epsilon$  (3.25 eV/atom).

$$N = 3$$

The two previously discussed triangles (Fig. 2) were the only mechanically stable structures available to  $\text{Si}_3$ . Without ambiguity, the equilateral triangle and isosceles triangle, consisting of only two bonds forming a perfect tetrahedral angle, may be referred to below as the triangle and chain, respectively. At low temperatures, both structures are visited, while the relative distribution of underlying structure shifts more toward the chain with increasing temperatures. This can be seen in Fig. 17 where the number of visitations ( $N_v$ ) versus underlying potential-energy minima ( $E$ ) is plotted for three finite-temperature systems. In Fig. 18, the local potential-energy minimum re-

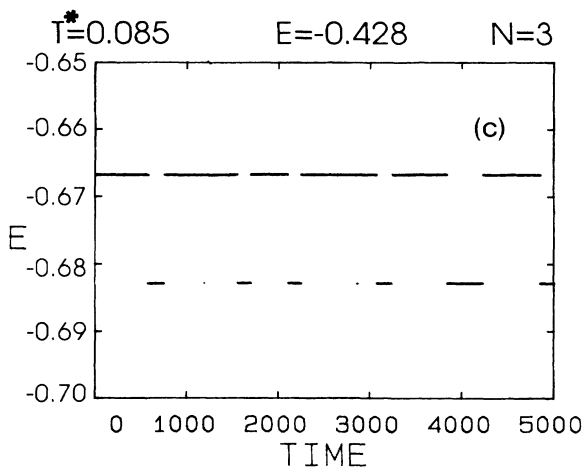
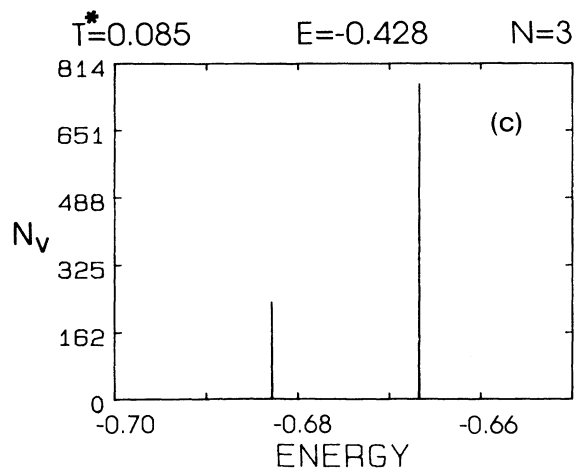
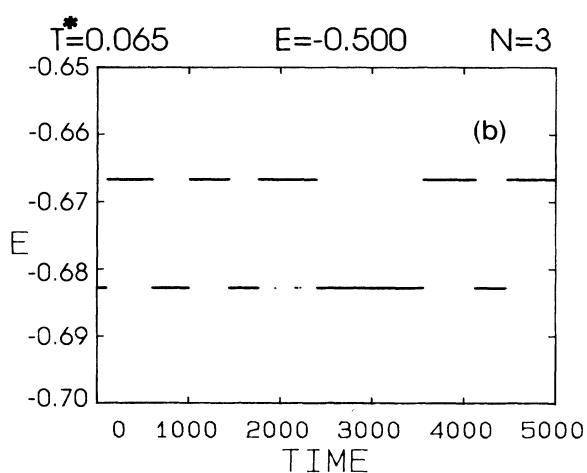
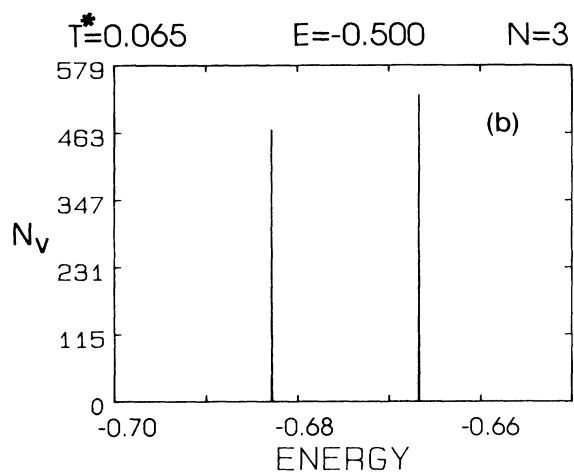
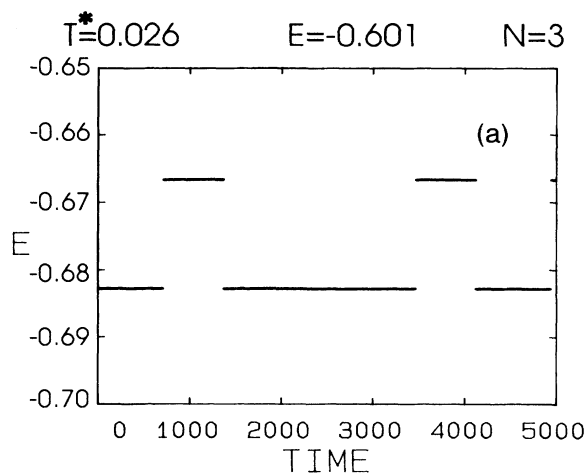
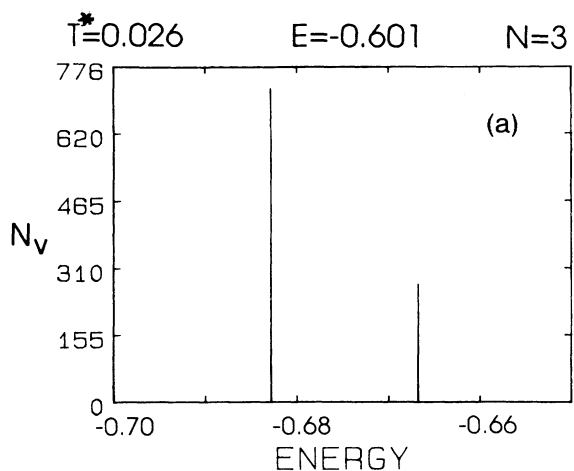


FIG. 17. Histograms of the visited potential minima for  $\text{Si}_3$  determined by 1000 SDQ mappings performed in parallel with a 5000 MD step simulation, see Fig. 1. Number of visitations  $N_v$  vs energy per atom ( $E$ ) after SDQ's are given for three different temperatures, (a)  $T^*=0.026$ , (b)  $T^*=0.065$ , and (c)  $T^*=0.085$ .

FIG. 18. Underlying potential minimum is plotted against the number of MD steps ( $\Delta t = 3.8 \times 10^{-16}$  sec) for the same three simulations depicted in Fig. 17. Not only does the majority of underlying state shift towards higher-energy configurations, but the frequency of transitions also increases with increasing temperature.

sulting from the SDQ is plotted against the MD time steps in order to show the frequency of transitions between the two structures. From this figure, one can see that not only does the majority of underlying states shift

towards higher-energy configurations, but the frequency of transitions also increases with increasing temperature. At  $T^* \sim 0.065$  both structures are equally likely to be visited. A step, similar to a structural transition, appears

near this energy in the graph of  $E$  versus  $T$  [Fig. 16(a)]. Recall  $T^* = 0.1$  corresponds to a temperature of 2500 K.

$$N = 4$$

Four structures and three energies, the highest one being doubly degenerate, are accessible to  $\text{Si}_4$ . Excluding the ground state, the structures listed in the order of increasing energy are the corner-shared triangle [Fig. 3(b)], the chain [Fig. 3(c)], and the trigonal pyramid [Fig. 3(d)]. The latter two geometries, fragments of the diamond structure, have three bonds with only tetrahedral angles and are therefore degenerate in energy. Corner-capped atoms added to the center or the end of the  $\text{Si}_3$  chain form the pyramid or chain, respectively. The two small jumps in the figure for  $E$  versus  $T$  [Fig. 16(b)], which appear at  $T^* \sim 0.07$  and 0.11, indicate changes in the most common underlying structure, first from the ground state to the corner-capped triangle and then to the high-energy structures, as depicted in the three histograms of Fig. 19.

$$N = 5$$

Of the seven energies found for configurations of  $\text{Si}_5$ , the energy of the squashed trigonal bipyramid [Fig. 4(b)] is the closest to that of the ground-state structure, a regular pentagon [Fig. 4(a)]. Another intermediate-energy configuration can be obtained by corner-capping the square [Fig. 4(c)]. Three high-energy structures can be viewed as corner-capping a triangle with a two-atom chain [Fig. 4(d)], corner-sharing two triangles and capping two atoms on the same corner of a triangle [Fig. 4(e)], both minor reconstructions of the crystalline tetrahedron. These last two structures are the first to appear with a fourfold-coordinated atom. The chain [Fig. 4(f)] and the tetrahedral fragment of the diamond lattice have the same highest energy with four bonds, but only the chain has been observed. The center atom of the tetrahedron is fourfold coordinated, but the remaining four atoms have only one bond and therefore the structure is unstable with respect to thermal fluctuations. Unlike  $\text{Si}_3$  and  $\text{Si}_4$ , the ground-state structure is dominant in the underlying structures even up to  $0.95E_f$ .

$$N = 6$$

Sixteen different potential-energy minima were found for  $\text{Si}_6$ , but only subsets of these structures were actually visited at any particular temperature. The lowest-energy structure [Fig. 5(a)], two equilateral triangles stacked in the form of a wedge, was not observed in systems near the fragmentation energy where more open structures were commonly found. A distorted octahedron, similar to that of RL and TS, is found, although a corner-capped pentagon [Fig. 5(c)] is closer in energy to the ground state and more frequently visited. Even at relatively low temperatures ( $T^* \sim 0.037$ ), the cluster undergoes many transitions between configurations of nearly equal energies. The three most commonly found geometries at  $0.95E_f$ , as determined by SDQ, were (i) the corner-capped pentagon, (ii) a two-atom chain attached to the corner of the square [Fig. 5(d)] and (iii) the capping of diagonally opposite

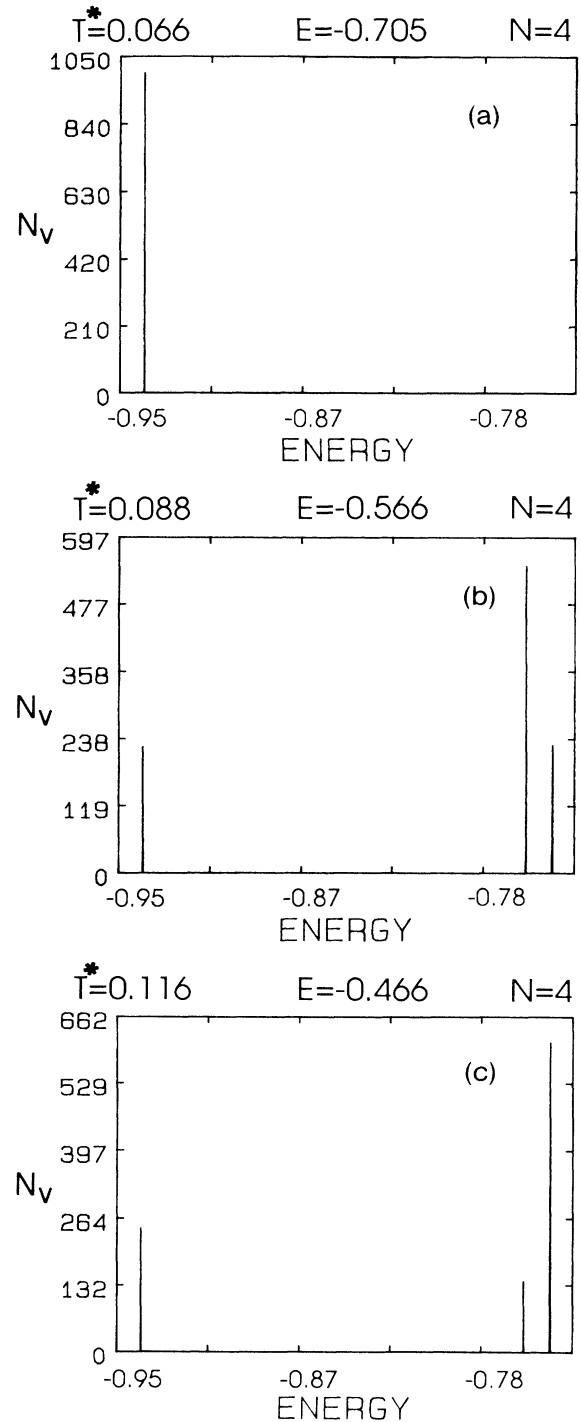


FIG. 19. Histograms of the visited potential minima for  $\text{Si}_4$  at (a)  $T^* = 0.066$ , (b)  $T^* = 0.088$ , and (c)  $T^* = 0.116$ .

corners of the square to form a distorted tetragonal bipyramid. It has been noted previously<sup>12</sup> that the tetragonal bipyramid is topologically similar to the six-membered "chair" ring though the energy corresponding to this microcrystalline fragment was seldom found from the steepest-descent mappings. The  $\text{Si}_6$  chain was found only

at the highest temperatures. The appearance of two small steps in the figure for  $E$  versus  $T$  [Fig. 16(d)] at  $T^* \sim 0.07$  and 0.11 concur with the histograms in Fig. 20, indicating the move of the majority of underlying states to higher-energy structures. These transitions are between three groups of structures [shown in Fig. 20(c)] and not just between single structures.

$$N = 7$$

The most commonly found low-energy configuration for  $\text{Si}_7$ , only 0.1% higher in energy than the ground state, is shown in Fig. 6(b). The other 22 structures found can be described by various edge sharings and cappings of the triangle, square, and pentagon. A dimer attached across a distorted pentagon's face [Fig. 6(c)] and a square sharing an edge with a pentagon [Fig. 6(d)] accounted for over 50% of the underlying mechanically stable structures at energies near  $E_f$ . The  $E$  versus  $T$  plot [Fig. 16(e)] has none of the interesting features exhibited by the smaller clusters, due to the large number of accessible configurations with an even distribution of binding energies.

$$N = 8$$

The  $\text{Si}_8$  ground-state geometry, a perfect cube [Fig. 7(a)], is a particularly stable structure since all atoms are threefold coordinated and all angles are at  $90^\circ$ , differing by  $19^\circ$  from the perfect tetrahedral angle. However, in our calculation [see Figs. 21(a) and 21(b) and discussion below] and in the experimental results, it is obvious that  $N = 8$  is not a magic number. This is an example of our assertion that  $E_0$  versus  $N$  (Fig. 15) cannot predict the existence of magic numbers. At approximately  $0.95E_f$ , the three configurations shown in Figs. 7(b)–7(d) account for almost 50% of the underlying stable structures while the ground state is no longer visited.

$$N = 9$$

The ground-state structure of  $\text{Si}_9$  [Fig. 8(a)] is the only one visited for energies upwards to  $0.5E_f$  and remains the dominant underlying structure for all energies under  $E_f$ . The only other structures to commonly appear are shown in Figs. 8(b) and 8(c).

$$N = 10$$

The ground-state configuration of two stacked pentagons [Fig. 9(a)] is visited in all systems of energies below  $E_f$ , though its presence decreases from 70% at  $0.5E_f$  to 8% at  $0.95E_f$ . At the latter energy, a particularly open structure containing one singly bonded atom was also present in 7% of the visited structures. The low-energy configuration in Fig. 9(b) was found 10% of the time, while the other 58 structures ranged from 0.2 to 8%. The two higher-energy structures shown in Figs. 9(c) and 9(d) were commonly found at finite temperatures. A five-membered ring, an irregular pentagon, is the basic subunit underlying all these structures.

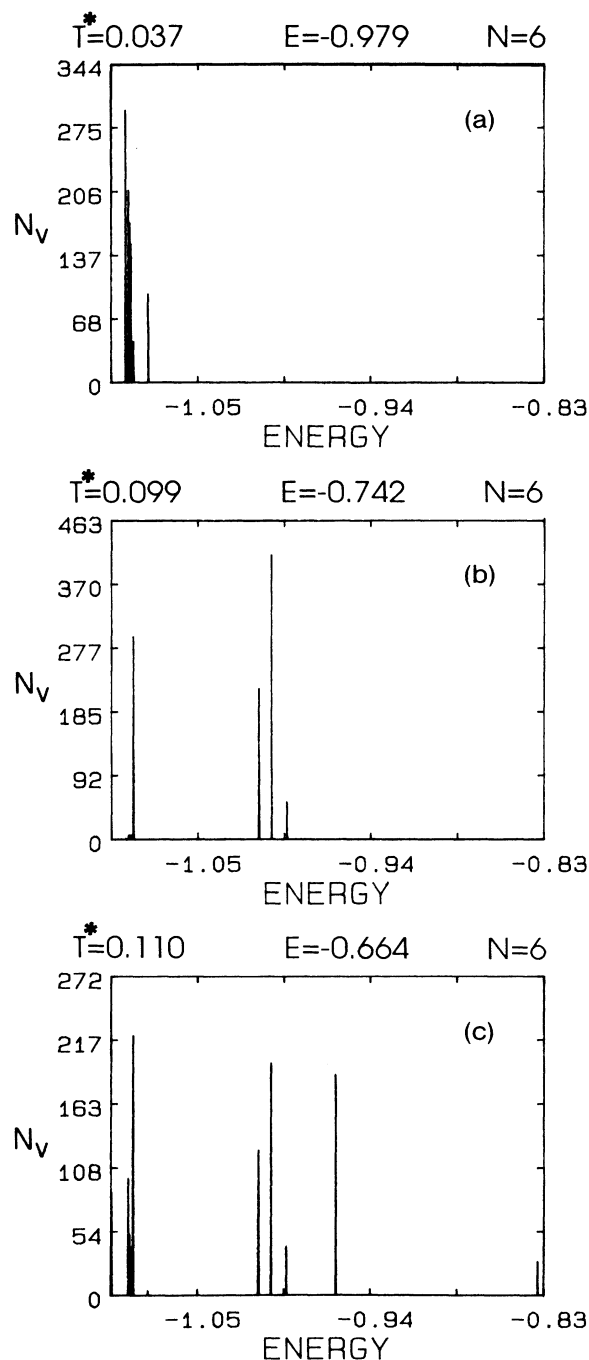


FIG. 20. Histograms of the visited potential minima for  $\text{Si}_6$  at (a)  $T^* = 0.037$ , (b)  $T^* = 0.099$ , and (c)  $T^* = 0.110$ . The structures accessible to  $\text{Si}_6$  can be grouped into sets of configurations of nearly equal energies. Transitions between subgroups occur with increasing temperature, indicated by the small jumps in  $E$  vs  $T$  [Fig. 16(c)].

$$N = 11$$

At high energies, the two lowest-energy structures for  $\text{Si}_{11}$  [Figs. 10(a) and 10(b)] account for only 2% of the underlying structures, while the most common geometry

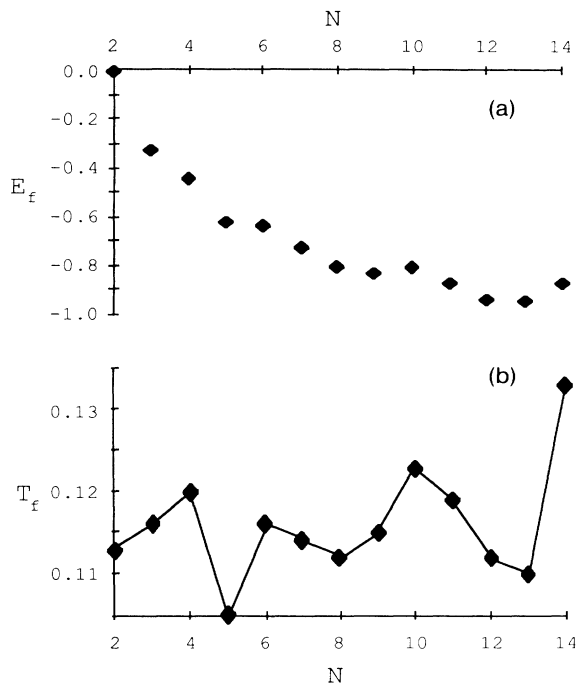


FIG. 21. (a) Fragmentation energy per atom ( $E_f$ ) vs number ( $N$ ); (b) fragmentation temperature ( $T_f$ ) vs number ( $N$ ). Peaks in these curves at  $N=4,6,10$  (magic numbers), clearly indicate the particular stability of the  $\text{Si}_{4,6,10}$  microclusters at high energies and temperatures. Fragments of these sizes were reported to be unusually common in the photofragmentation experiment of Bloomfield, Freeman, and Brown (Ref. 12).

[Fig. 10(c)] is found less than 6% of the time. The high-temperature cluster frequently alters its form between the 74 available structures. Most, if not all, of these structures may be constructed by various surface packings of four- and five-sided nonplanar faces. The number of visitations  $N_v$  versus potential-energy minima  $E$ , shown in Figs. 22(a)–22(d), are seen to be evenly distributed over a wide range of energy. In Figs. 22(e) and 22(f) the transitions between accessible potential-energy minima are shown to increase with increasing temperature. These latter two graphs show that the transition between low- and high-energy structures involves many intermediate configurations resulting in a relatively smooth  $E$  versus  $T$  curve [Fig. 16(i)].

$N=12$

Only 54 potential-energy minima were identified for  $\text{Si}_{12}$ , with the ground state [Fig. 11(a)] forming a common underlying structure for all energies below  $E_f$ . Even though all atoms are threefold coordinated in this structure, fully bonded fourfold-coordinated atoms appear in some of the higher-energy configurations [see Fig. 11(d)]. The low-energy structure shown in Fig. 11(b) was also commonly found at high temperatures. All stable configurations are accessible at  $0.95E_f$ , with the ground state remaining the most common at 20% of the steepest-

descent mapped minima. The only other configuration visited more than 10% of the time at this high energy is shown in Fig. 11(c).

$N=13$

Two low-energy structures other than the ground state [Fig. 12(a)] are commonly found at finite temperatures. The more stable of these two high-energy structures has two fully bonded fourfold-coordinated atoms with two five-membered rings and one three-membered ring in addition to the six four-membered rings [Figs. 12(b)], while the other structure has only three bonds per atom with a surface formed by six five-membered rings and two four-membered rings [Fig. 12(c)]. These three low-energy configurations account for 50% of the underlying structures at  $0.75E_f$  and 5% at  $0.95E_f$ . Close to  $E_f$ , nearly 70 of the 95 identified potential minima are visited, but none seems to be preferred, with the most common appearing less than 6% of the time.

$N=14$

For energies on the order of  $0.25E_f$ , all atoms vibrate about the  $\text{Si}_{14}$  ground-state equilibrium positions [Fig. 13(a)], but structural transformations occur for higher energies and the lowest-energy configuration accounts for less than 1% of the visited structures. In total, 156 potential-energy minima have been found that span the energy range of  $0.24\epsilon$  between lowest and highest energies. The majority of these structures is best seen as the many possible combinations of taking four- and five-sided figures to form a closed structure [Figs. 13(b) and 13(c)].

## VI. MAGIC NUMBERS

The results of the present MD simulation indicate that four-, six-, and ten-atom clusters are relatively stable structures at temperatures on the order of the melting temperature. Curves of fragmentation energy per atom ( $E_f$ ) and fragmentation temperature ( $T_f$ ) versus number ( $N$ ) are shown in Figs. 21(a) and 21(b), respectively. The fragmentation energy was determined from approximately 60 systems generated for each cluster  $\text{Si}_{3-14}$ . The fragmentation temperature was found from averaging the kinetic energy over 25 000 MD time steps for the system with energy  $E_f$ . Peaks in the curve for  $E_f$  versus  $N$  clearly indicate that six- and ten-atom microclusters have particularly stable high-energy configurations, while the peak at  $N=4$  is not so apparent. However, sharp peaks do appear in the  $T_f$  versus  $N$  curve for the three experimentally determined magic numbers  $N=4, 6$ , and  $10$ . It is also obvious in both curves that  $\text{Si}_{14}$  is very stable at high temperatures with respect to  $\text{Si}_{13}$ . There has not been an experimental investigation of the relative stability of  $\text{Si}_{14}$ , but Martin and Schaber<sup>13</sup> have found  $N=14$  to be a magic number for Ge. The ground-state energy per atom ( $E_0$ ) found through the SDQ mapping is given with the fragmentation energy per atom ( $E_f$ ) and temperature ( $T_f$ ) for  $\text{Si}_{2-14}$  in Table I.

The most common structures of  $\text{Si}_6$  and  $\text{Si}_{10}$  at energies near  $E_f$  both contain a single atom capped to a pentagon.

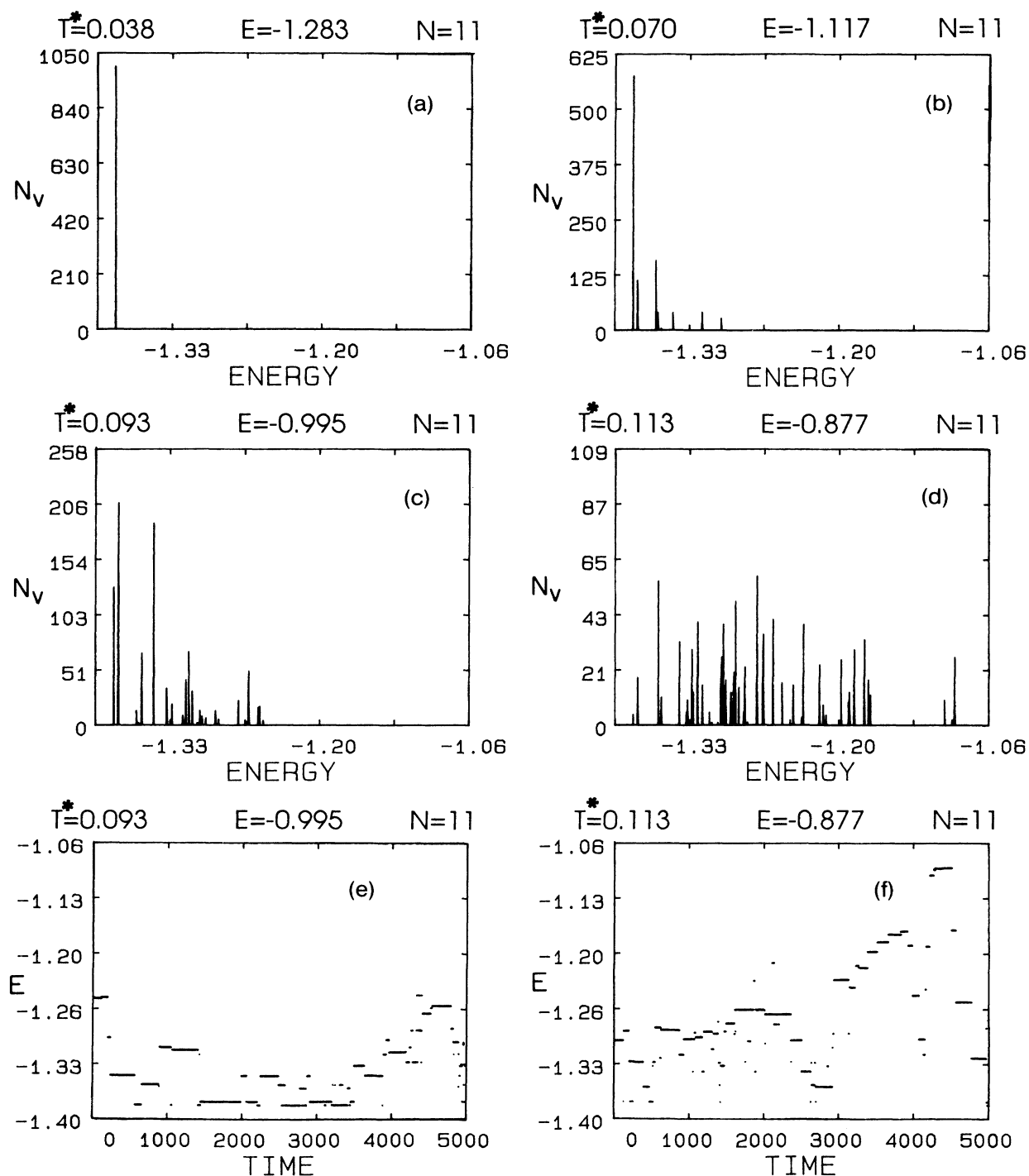


FIG. 22. Histograms of the visited potential minima for  $\text{Si}_{11}$  at (a)  $T^* = 0.038$ , (b)  $T^* = 0.070$ , (c)  $T^* = 0.093$ , and (d)  $T^* = 0.113$ . The underlying potential minimum is plotted against the MD time step for the highest two temperatures in (e) and (f). The transitions between high- and low-energy structures are shown to involve many intermediate structures.

Each atom in the pentagon has a considerable degree of freedom similar to the local environment of an atom in a high-energy chain, but with a small additional contribution to the potential energy due to the three-body interaction. It appears to be the ability of the  $\text{Si}_6$  and  $\text{Si}_{10}$  clus-

ters to access these low-energy, loosely bound structures containing one single atom bonded to five-membered rings that enables them to remain stable at relatively high temperatures.

The most common channel for all  $\text{Si}_N$  ( $N = 2-14$ ) is



TABLE I. The zero-temperature ground-state energy  $E_0$  per atom, fragmentation energy per atom  $E_f$ , and the corresponding fragmentation temperature  $T_f$  for  $\text{Si}_{2-14}$ .

Number $N$	Minimum	Fragmentation	
	energy $E_0$	Energy $E_f$	Temp. $T_f$
2	-0.5000	0.000	0.113
3	-0.6828	-0.326	0.116
4	-0.9386	-0.449	0.120
5	-0.9996	-0.620	0.105
6	-1.0906	-0.632	0.116
7	-1.1788	-0.726	0.114
8	-1.3223	-0.807	0.104
9	-1.3271	-0.835	0.115
10	-1.3797	-0.803	0.123
11	-1.3829	-0.870	0.119
12	-1.4178	-0.934	0.112
13	-1.4234	-0.945	0.110
14	-1.4455	-0.866	0.133

the fragmentation into  $\text{Si} + \text{Si}_{N-1}$ . When the parent cluster separates into two or more compact subunits connected by single bonds before fragmentation, then nontrivial fragments can result. As an example,  $\text{Si}_4$  can only fragment into  $\text{Si}_2 + \text{Si}_2$  by severing the center bond of the  $\text{Si}_4$  chain. The relative probability of the cluster  $\text{Si}_N$  dissociating into the fragments  $\text{Si}_{N-M} + \text{Si}_M$  ( $M=1,2,3,4$ ) is given in Table II.  $\text{Si}_3$  is found to dissociate into one- and two-atom fragments from the chain at  $T^*=0.116$ . Fragmentation of  $\text{Si}_4$  can occur from any configuration except the ground state, with the pyramid being the most likely to fragment. Even though the pentagon is the most common underlying configuration for  $\text{Si}_5$ , near  $E_f$  the cluster decomposes into one- and four-atom fragments. This usually occurs from either the corner-capped square or a triangle capped with a two-atom chain. The latter configuration can decompose into  $\text{Si} + \text{Si}_4$  or  $\text{Si}_2 + \text{Si}_3$  by severing one bond. For  $\text{Si}_{2-7}$ , the reported primary fragmenta-

TABLE II. Primary channels of fragmentation for  $\text{Si}_{2-14}$  as determined from 20–30 events for each size cluster. Fragmentation from  $\text{Si}_N$  to  $\text{Si}_{(N-2)} + \text{Si}_2$  indicates the  $\text{Si}_{4,6,10}$  are particularly common fragments, while the fragmentation from  $\text{Si}_N$  to  $\text{Si}_{(N-3)} + \text{Si}_3$  supports the common occurrence of  $\text{Si}_4$  and  $\text{Si}_6$  fragments.

$N$	$(N-1)+1$	$(N-2)+2$	$(N-3)+3$	$(N-4)+4$
2	1.00			
3	1.00			
4	0.90	0.10		
5	0.82	0.18		
6	0.64	0.25	0.11	
7	0.62	0.19	0.19	
8	0.55	0.35	0.05	0.05
9	0.64	0.12	0.16	0.08
10	0.74	0.22	0.00	0.04
11	0.65	0.15	0.10	0.10
12	0.70	0.25	0.05	0.00
13	0.76	0.12	0.04	0.08
14	0.76	0.14	0.00	0.10

tion channels are in accord with the results of BFB. Experimentally, the larger clusters were seen to dissociate into fragments containing predominantly  $\text{Si}_6$  remnants. Whether these final states are the results of primary or multiple fragmentation events is unknown. In the present simulation, configurations from which fragmentation occurred for  $\text{Si}_{6-14}$  clusters usually consisted of a parent cluster made up of smaller, compact clusters connected through single bonds. In more than 50% of the fragmentation events, one such subgroup contained only one atom which was the cause of fragmentation.

Evidence for the stability of the magic numbers is also found in the nontrivial fragmentation channels  $N \rightarrow 2 + (N-2)$  and  $N \rightarrow 3 + (N-3)$ . The  $\text{Si}_{6,8,12}$  clusters were observed to have the highest probability of nontrivial fragmentation, with at least 25% of the observed events resulting in  $\text{Si}_2 + \text{Si}_{4,6,10}$ , respectively [see Table II, column titled “ $(N+2)-2$ ”].  $\text{Si}_{7,9}$  clusters were also found to have a large probability of dissociating into  $\text{Si}_3$  and  $\text{Si}_{4,6}$  [see Table II, column titled “ $(N-3)-3$ ”]. These relatively high probabilities for nontrivial fragmentation into four-, six-, and ten-atom clusters are in good agreement with the experimental fragmentation spectra and support the claim for the unusual stability of  $\text{Si}_{4,6,10}$  microclusters. Since the previous quantum-chemical calculations have found nearly the same structure for both neutral and charged Si clusters, it is probable that thermally driven fragmentation would also result in similar spectra.

From the ground-state energy ( $E_0$ ) versus number ( $N$ ) curve [Fig. 15(a)] it is apparent that  $\text{Si}_4, \text{Si}_6$ , and  $\text{Si}_{10}$  do not form unusually stable clusters. Thus knowledge of the zero-temperature ground-state structures is not sufficient to explain the existence of the experimentally observed magic numbers for silicon clusters described by the SW potential. However, the magic numbers clearly do appear in the finite-temperature results. The fragmentation energy ( $E_f$ ) and temperature ( $T_f$ ) indicate the  $\text{Si}_4, \text{Si}_6$ , and  $\text{Si}_{10}$  are particularly stable clusters at high temperatures, on the order of the melting temperature. This is consistent with the experimental situation where clusters fragment from high-energy configurations. The fragmentation spectra further indicate that  $\text{Si}_{4,6,10}$  are particularly stable. The angles, bond lengths, and structures found for each cluster are a direct result of the SW potential and could change with further improvements. However, we believe that the SW three-body potential describes correctly the essential features of the energetics and fragmentation of silicon microclusters. Many of the results described above will be common to germanium clusters.

*Note added.* The recently completed study by E. Blaisten-Barojas and D. Levesque used the SW potential to determine the ground-state structures of neutral and charged silicon microclusters through molecular-dynamic quenching (MDQ).<sup>36</sup> By slowly scaling the atomic velocities to zero from some high-temperature equilibrium state, one expects to find the ground state of the cluster. The lowest-energy structures obtained from this method for neutral clusters differ from those determined by the SDQ technique for  $\text{Si}_6, \text{Si}_{11}$ , and  $\text{Si}_{13}$ . In Ref. 36, Fig. 5, the lowest-energy configurations found from MDQ are shown

for  $\text{Si}_{3-17}$ . All structures given for  $\text{Si}_{3-14}$  were found in the present SDQ study, yet for  $\text{Si}_6$ ,  $\text{Si}_{11}$ , and  $\text{Si}_{13}$ , lower-energy structures were also discovered. The structures in Ref. 36 for  $\text{Si}_6$ ,  $\text{Si}_{11}$ , and  $\text{Si}_{13}$  are shown in Figs. 5(b), 10(b), and 12(b), respectively. The configurations corresponding to the global minima [Figs. 5(a), 10(a), and 12(a)] have less than 1% higher binding energy than those found from MDQ. In these three cases we have found many structures with binding energies close to that of the ground state. The authors also claim that 6-, 10-, and 14-atom clusters do not allow the formation of six-membered rings, but our SDQ results have found all clusters  $\text{Si}_N$ ,  $N \geq 6$ , to contain six-membered rings in some of their high-energy structures. Simulation of charged clusters was attempted through the addition of a one-body term to the SW potential. This term assumed an isotropic polarizability for each atom and did not distinguish between positively or negatively charged clusters. The ground-state structures for  $\text{Si}_N$  ( $N \geq 5$ ) were very different

from the neutral cluster results, with the charged atom usually sitting in the center of a tetrahedron with four bonds. We recall that the results of the quantum-chemical calculation of RL and TS indicate that the charged atom was the least bonded in the cluster and that the binding energies were slightly higher than the neutral clusters, in direct conflict with these authors findings.

#### ACKNOWLEDGMENTS

One of the authors (B.P.F.) would like to acknowledge financial support from the Department of Educational Programs, Argonne National Laboratory, and the hospitality of the Material Science and Technology Division at Argonne National Laboratory. Work was supported by the U.S. Department of Energy (Office of Basic Energy Science, Division of Materials Science), under contract No. W-31-109-Eng-38.

\*Address up to 31 August 1987: Laboratory of Atomic and Solid State Physics, Clark Hall, Cornell University, Ithaca, NY 14853-2501.

<sup>1</sup>R. Van Hardeveld and F. Hartog, *Adv. Catal.* **22**, 75 (1975).

<sup>2</sup>W. D. Knight, K. Clemenger, W. A. de Heer, W. A. Saunders, M. Y. Chou, and M. L. Cohen, *Phys. Rev. Lett.* **52**, 2141 (1984).

<sup>3</sup>B. K. Rao, P. Jena, and M. Manninen, *Phys. Rev. B* **32**, 477 (1985); B. K. Rao and P. Jena, *ibid.* **32**, 2058 (1985); *J. Phys. F* **16**, 461 (1986).

<sup>4</sup>P. A. Montano, W. Schulze, B. Tesche, G. K. Shenoy, and T. I. Morrison, *Phys. Rev. B* **30**, 672 (1984); P. A. Montano, G. K. Shenoy, E. E. Alp, W. Schulze, and J. Urban, *Phys. Rev. Lett.* **56**, 2076 (1986).

<sup>5</sup>M. R. Hoare and P. Pal, *Adv. Phys.* **20**, 161 (1971).

<sup>6</sup>F. F. Abraham, *Rep. Prog. Adv. Phys.* **45**, 1113 (1982).

<sup>7</sup>O. Echt, K. Sattler, and E. Recknagel, *Phys. Rev. Lett.* **47**, 1121 (1981).

<sup>8</sup>P. W. Stephens and J. G. King, *Phys. Rev. Lett.* **51**, 1538 (1983).

<sup>9</sup>I. A. Harris, R. S. Kidwell, and J. A. Northby, *Phys. Rev. Lett.* **53**, 2390 (1984).

<sup>10</sup>R. E. Honig, *J. Chem. Phys.* **22**, 1610 (1954).

<sup>11</sup>T. T. Tsong, *Phys. Rev. B* **30**, 4946 (1984).

<sup>12</sup>L. A. Bloomfield, R. R. Freeman, and W. L. Brown, *Phys. Rev. Lett.* **54**, 2246 (1985).

<sup>13</sup>T. P. Martin and H. Schaber, *J. Chem. Phys.* **83**, 855 (1985).

<sup>14</sup>J. R. Heath, Y. Lin, S. C. O'Brien, Q. L. Zhang, R. F. Curl, R. E. Smalley, and F. K. Tittel, *J. Chem. Phys.* **83**, 5520 (1985).

<sup>15</sup>K. Raghavachari and V. Logovinsky, *Phys. Rev. Lett.* **55**, 2853 (1985).

<sup>16</sup>D. Tománek and M. A. Schlüter, *Phys. Rev. Lett.* **56**, 1055 (1986).

<sup>17</sup>J. Farges, M. F. Feraudy, B. Raoult, and G. Torchet, *J. Chem. Phys.* **78**, 5067 (1983).

<sup>18</sup>E. A. Rohlfing, D. M. Cox, and A. Kaldor, *J. Chem. Phys.* **81**, 3322 (1984); B. K. Rao, S. N. Khanna, and P. Jena, *Solid*

*State Commun.* **58**, 53 (1986).

<sup>19</sup>S. Saito, S. Ohnishi, and S. Sugano, Technical Report of The Institute of Solid State Physics, University of Tokyo, Ser. A. p. 1608, 1985 (unpublished).

<sup>20</sup>M. M. Francl, W. J. Pietro, W. J. Hehre, J. S. Binkley, M. S. Gordon, D. J. DeFrees, and J. A. Pople, *J. Chem. Phys.* **77**, 3654 (1982).

<sup>21</sup>R. Krishnan, M. J. Frisch, and J. A. Pople, *J. Chem. Phys.* **72**, 4244 (1980).

<sup>22</sup>W. Kohn and P. Vashishta, in *Theory of the Inhomogeneous Electron Gas*, edited by S. Lundquist and N. H. March (Plenum, New York, 1983), Chap. 2.

<sup>23</sup>P. Hohenberg and W. Kohn, *Phys. Rev.* **136**, B864 (1964).

<sup>24</sup>W. Kohn and L. J. Sham, *Phys. Rev.* **140**, A1133 (1965).

<sup>25</sup>D. J. Chadi, *Phys. Rev. B* **29**, 785 (1984).

<sup>26</sup>K. Binder and M. H. Kalos, in *Monte Carlo Methods in Statistical Physics*, edited by K. Binder (Springer, New York, 1979), Chap. 6.

<sup>27</sup>J. W. Moskowitz, K. E. Schmidt, M. A. Lee, and M. H. Kalos, *J. Chem. Phys.* **77**, 349 (1982).

<sup>28</sup>D. M. Ceperley and E. L. Pollock, *Phys. Rev. Lett.* **56**, 351 (1986).

<sup>29</sup>S. Kirkpatrick, C. D. Gelatt, Jr., and M. P. Vecchi, *Science* **220**, 671 (1983).

<sup>30</sup>R. Car and M. Parrinello, *Phys. Rev. Lett.* **55**, 2471 (1985).

<sup>31</sup>A. Rahman, in *Correlation Functions and Quasiparticle Interaction in Condensed Matter*, Vol. 35 of *NATO Advanced Studies Series*, edited by J. Woods Halley (Plenum, New York, 1977).

<sup>32</sup>F. H. Stillinger and T. A. Weber, *Phys. Rev. B* **31**, 5262 (1985).

<sup>33</sup>D. Beeman, *J. Comp. Phys.* **20**, 130 (1976).

<sup>34</sup>F. H. Stillinger and T. A. Weber, *Phys. Rev. A* **28**, 2408 (1983); *Science* **225**, 983 (1984).

<sup>35</sup>D. J. Chadi, *Phys. Rev. B* **32**, 6485 (1985).

<sup>36</sup>E. Blaisten-Barojas and D. Levesque, *Phys. Rev. B* **34**, 3910 (1986).